# Control of Air Bubble Cluster by a Vortex Ring Launched into Still Water

Tomomi Uchiyama and Sou Kusamichi

***Abstract*—An experimental study searching for the possible generation and transport of a bubble cluster by a vortex ring in water is performed. A vortex ring is launched vertically upward into a water tank by discharging the water from a cylinder mounted at the bottom of the tank with a piston. Air bubbles are successively injected into the vortex ring from a needle attached to the cylinder outlet. The cylinder inner diameter $D_0$ and the piston stroke $L_0$ are 42.5 mm and 100 mm, respectively. The circulation of the vortex ring is less than 20000, and accordingly laminar vortex rings are launched. The mean diameter of the bubbles is 3.4 mm. The generation of bubble cluster and transport of the cluster by the vortex ring can be classified into four patterns according to the piston velocity (strength of the vortex ring) and the air volumetric flow rate. When the strength of the vortex ring is low, the bubbles are less affected by the vortex ring and instead rise with the buoyant force at a higher velocity than the vortex ring. With an increase in the strength of the vortex ring, the bubbles are entrained in the vortex core and form a cluster. The bubbles entrained in the vortex core circumferentially disperse around the vertical axis of the vortex ring, and they are successfully transported by the convection of the vortex ring. The convection velocity of the vortex ring is scarcely affected by the entrained bubbles, but the radius is enlarged slightly. The circulation of a vortex ring that entrains and transports air bubbles in this study is nearly accurately predicted by the formula of Milenkovic et al., which gives the circulation of a vortex ring entraining a single bubble in the vortex core.**

***Index Terms*—Bubble cluster, bubble entrainment, vortex ring, vorticity, visualization.**

## I. Introduction

A vortex ring is characterized by two motions. The first motion is the vortical motion around the vortex core forming a closed circle, and the second motion is the resultant convection motion in the direction perpendicular to the plane of the circle. The vortex ring entrains matter in the vortex core with the vortical motion and transports the entrained matter with the convection motion. The entrainment and transport of solid particles by a vortex ring have been investigated [1], [2]. Domon *et al.* [1] conducted an experimental study on the transport of spherical particles in water. In their experiment, a vortex ring was loaded with resin particles of a specific weight 1.02 and mean diameter 0.4 mm at the launch into still water. The behavior of the vortex ring and the particle motion were examined by the visualization. One of the authors [2] performed a numerical simulation of the convection of a vortex ring laden with small particles. The Stokes number St, which is defined as the ratio of the particle response time to the characteristic time of the vortex ring [3], was chosen as the simulation parameter. At the launch of the vortex ring into quiescent air, spherical particles were arranged on the cross-section of the vortex ring. The simulation at St = 0.01 highlighted that the vortex ring involves the particles at the launch and that it can transport the particles with the convection. The simulation also clarified the effect of St on the behavior of the vortex ring and the particle motion.

Small gas bubbles in a liquid flow preferentially distribute around the high-vorticity region [4], [5]. Since a vortex ring is composed of a circular vortex core where the vorticity is highly concentrated, it may successfully entrain small bubbles in the vortex core and transport the entrained bubbles via the convection. However, these vortex ring abilities have not been investigated. The interactions between the bubbles and a vortex ring would play an important role in bubble entrainment and transport. Research on such interactions has scarcely been reported except for the studies of Sridhar and Katz [6], [7] and Higuera [8], which investigated the motion of a single bubble in a vortex core and the bubble-induced deformation of a vortex ring. Thus, the current authors [9-12] researched possible entrainment and transport of small bubbles by a vortex ring. Uchiyama [9] conducted a numerical simulation of a water jet laden with small air bubbles and showed that a vortex ring induced near the nozzle outlet by an axisymmetric disturbance involves the bubbles and convects with the bubbles along the jet centerline. Uchiyama and Yoshii [10] simulated the bubble motion and the behavior of a vortex ring launched toward a bubble cluster, and they demonstrated the entrainment and transport of the bubbles by the vortex ring as well as the change in the strength of the vortex ring because of the entrained bubbles. Wang *et al.* [11] simulated the interaction between a bubble plume and a vortex ring and reported the effect of the bubbles on the behavior of the vortex ring. Uchiyama and Kusamichi [12] performed an experimental study to explore the interaction between a bubble cluster and a vortex ring. Small hydrogen bubbles were generated by water electrolysis at the bottom of a water tank. The bubbles rise owing to the buoyancy force in water, which induces a bubble plume. A vortex ring was launched vertically upward into the bubble plume. The diameter and velocity of the vortex ring convecting in the bubble plume, the bubble motion, and the water velocity distribution were measured. The experiment highlighted the bubble entrainment in the vortex core and the change in the convection of the vortex ring because of the entrained bubbles.

Manuscript received July 1, 2016; revised October 12, 2016.

T. Uchiyama is with Institute of Materials and Systems for Sustainability, Nagoya University, Nagoya 464-8603, Japan (e-mail: uchiyama@is.nagoya-u.ac.jp).

S. Kisamichi is with Bridgestone Cycle Co., Ltd, Ageo 362-0072, Japan.

The previously mentioned pioneering works of the current authors [9]-[12] demonstrated that a vortex ring can be successfully employed for the control of bubble motion or the entrainment and transport of bubbles if the strength and scale of the vortex ring are set appropriately. Active control of bubble motion is a component technology applicable to the drive, supply, and removal of bubbles dispersed in liquid. Thus, it would be a widely utilized technology in various engineering applications. The drive and supply of bubbles can accurately regulate the mixing and chemical reaction between bubbles consisting of different kinds of gases. They are also favorably used to the washing of a precision machinery component with small amounts of bubbles. The removal of bubbles enables the control of heat transfer, because the vapor bubbles generated on a heating surface govern the rate of heat transfer to the liquid-phase. Thus far, bubble control methods using an ultrasonic wave [13] and a swirling flow [14] have been presented. However, the ultrasonic wave method is limited to only a single bubble and the swirling flow method cannot accurately control bubble motion. A control method using a vortex ring can be expected to simultaneously solve these problems. The strength of the vortex ring and the amount of bubbles around the vortex ring would affect the performance of the control method. But such effects were not fully investigated by the authors' previous works.

The objective of this study is to experimentally search for a method to control bubble clusters. In this method, a vortex ring entrains the desired number of bubbles in the vortex core to generate the bubble cluster, and it effectively transports the bubble cluster to a fixed location via the convection. A vortex ring launcher, composed of a cylinder and a piston, is mounted at the bottom of a water tank, and a vortex ring is launched vertically upward in the tank. Air bubbles are successively injected into the vortex ring from a needle attached to the cylinder outlet. The inner diameter of the cylinder is 42.5 mm. The circulation or the strength of the vortex ring is less than 20000, and the mean diameter of the bubble at the outlet of the bubble injection needle is 3.2 mm. The behavior of the vortex ring, the entrainment of the bubbles in the vortex core, and the motion of the entrained bubbles relative to the convecting vortex ring are explored. The effects of the circulation of the vortex ring and the air volumetric flow rate are elucidated.

## II. Experimental

### A. Experimental Set-up

Fig. 1 shows a schematic of the experimental set-up. The experiment is conducted in a water tank made of transparent acrylic resin. The width and depth of the tank are 300 mm, and the height is 600 mm. The top of the tank is open to the atmosphere. A vortex ring launcher, composed of a cylinder and a piston, is mounted at the bottom of the tank. The cylinder centerline is vertical, and the cylinder outlet is positioned above the bottom of the tank.

A vortex ring is launched vertically upward into the water tank by discharging the water in the cylinder with a piston. The push of the piston is performed by a slider connected to an AC servomotor. The velocity and stroke are controlled by a personal computer.

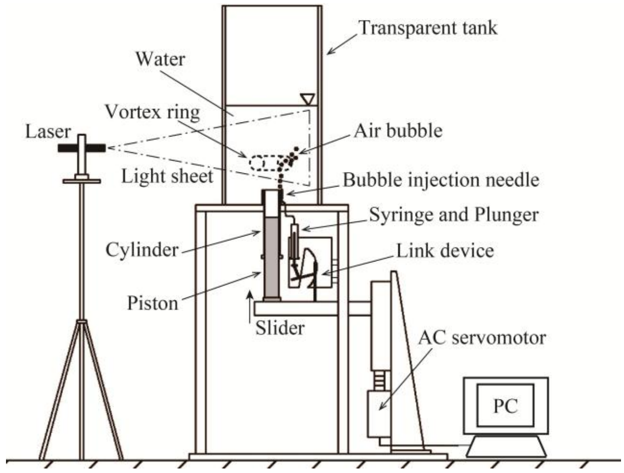


Fig. 1. Schematic diagram of experimental set-up.

A needle injecting air bubbles into the water is attached to the outer wall of the cylinder outlet. It is parallel to the cylinder axis, and the tip is positioned on the cylinder outlet. The bubble injection needle is connected to a syringe. Air in the syringe is fed to the needle via a plunger push and air bubbles are injected into the water tank. The push-up is also performed by the slider driving the vortex ring launcher. The motion of the slider is transmitted to the plunger via a link mechanism.

The image of the central vertical cross-section of the vortex ring is captured by a video camera using a laser light sheet (power: 100 mW, wavelength: 532 nm, thickness: 1 mm). The spatial resolution, frame rate, and shutter speed of the camera are 640 × 480 pixels, 200 fps, and 1/200 s, respectively. The water velocity is measured by a PIV system. Nylon particles (mean diameter: 80 μm, specific weight: 1.02) are used as the tracers. It is assumed that the particles scarcely affect the water velocity field.

### B. Launch of the Vortex Ring

Fig. 2 shows the close-up of the vortex ring launcher. The piston stroke $L_0$ is 100 mm, and the top dead center is positioned 46 mm below the cylinder outlet. The inner $D_0$ and outer diameters of the cylinder are 42.5 mm and 57.8 mm, respectively. The height of the cylinder outlet from the bottom of the tank is 45 mm. The origin of the vertical ($z$) and radial ($r$) axes is set at the center of the cylinder outlet. The water depth is 300 mm.

The experiment is conducted using the piston velocities $U_m$ listed in Table I. Fig. 3 shows the time variation of the displacement $z_p$ and velocity $U_0$ (= $dz_p/dt$) of the piston at $D_0U_m/\nu$ = 6630, 12900, and 19700, where $t^*$ is the non-dimensional time defined by $t(g/D_0)^{1/2}$ and $\nu$ is the kinematic viscosity of the water. The velocity profile is trapezoidal, and the maximum velocity $U_m$ is maintained for a specified period of time.

When a fluid is discharged from a cylinder into the still fluid by a piston, a laminar or turbulent vortex ring is launched depending on the discharge conditions. Glezer [15] identified the conditions that lead to generation of the laminar and turbulent vortex rings as shown in Fig. 4. The turbulent vortex ring is characterized by the active mixing just behind it.

The identification is based on the cylinder inner diameter $D_0$, the piston stroke $L_0$ and the circulation $\Gamma_0$ of the vortex ring. $\Gamma_0$ is computed from the following equation:

$$\Gamma_0 = \int_0^{T_0} \frac{U_0^2}{2} \mathrm{d}t \quad (1)$$

where $T_0$ and $U_0$ are the motion time and velocity of the piston, respectively. The values of $\Gamma_0$ for this study are plotted in Fig. 4. On the basis of identification by Glezer [15], it is determined that laminar vortex rings are launched.

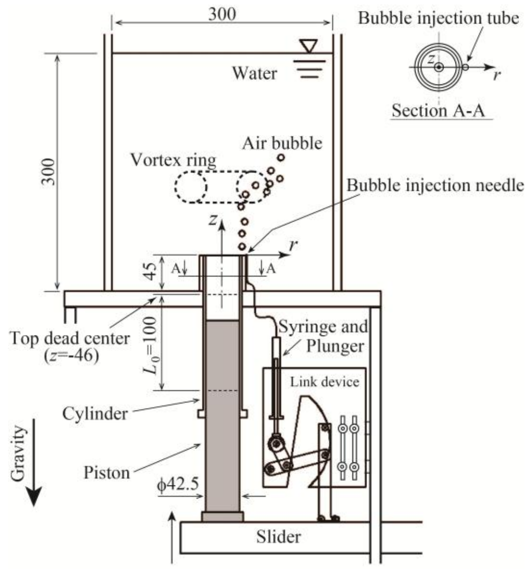


Fig. 2. Vortex ring launcher.

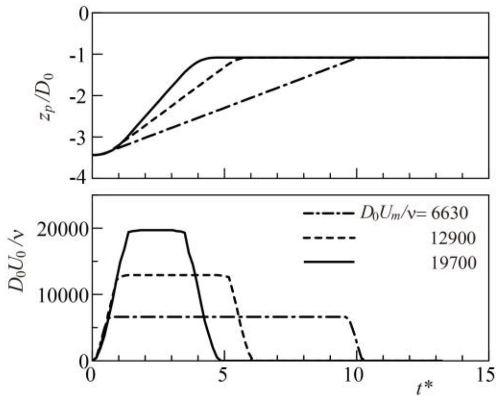


Fig. 3. Displacement and velocity profiles of piston.

TABLE I: EXPERIMENTAL CONDITIONS

| **Vortex ring** | |
|---|---|
| Inner diameter of cylinder, $D_0$ | 42.5 mm |
| Stroke of piston, $L_0$ | 100 mm |
| Maximum velocity of piston, $D_0U_m/\nu$ | 2125, 4250, 6630, 9560, 12900, 15900, 19700 |
| Circulation calculated by Eq. (1), $\Gamma_0/\nu$ | 2449, 4943, 7426, 10931, 13993, 16506, 19656 |
| **Air injection** | |
| Air volume, $Q_g/L_0D_0^2$ | 0.55, 1.11, 1.66, 2.21, 2.78 x $10^{-3}$ |
| Air volumetric flow rate, $\dot{Q}_g/D_0\nu$ | 1.18 - 38.0 |
| Mean bubble diameter, $\bar{d}_b$ | 3.4 mm |

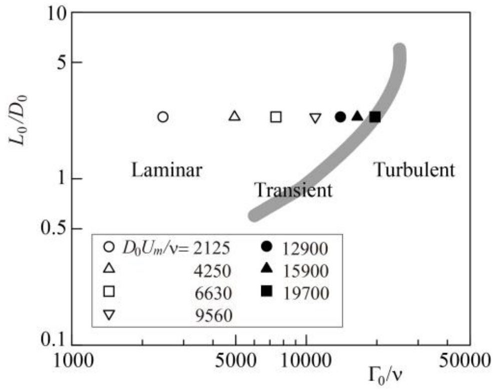


Fig. 4. Experimental condition for launch of vortex ring plotted on the identification map of Glezer (1988).

### C. Injection of the Air Bubbles

Fig. 5 shows a detailed view of the device injecting air bubbles into the water tank. A bubble injection needle made of stainless steel is attached to the outer wall of the cylinder outlet in due consideration that the largest shear force appears at the needle tip. The length and inner diameter of the needle are 20 mm and 0.26 mm, respectively. The needle is connected to a syringe via a thin polyethylene tube. The capacity of the syringe is 1000 mm$^3$. The syringe is mounted on a plate fixed at the support of the water tank. A plunger inside the syringe is pushed up by the slider used to launch the vortex ring. The motion of the slider is transmitted to the plunger via a link mechanism comprising three links. For Link 2, Joint 1 is fixed on the support plate; Joint 2 is connected with Link 1; and Link 3 is connected to Link 2 via Joint 3. The vertical motion of the slider is transmitted to the plunger through Links 1, 2, and 3. The position of Joint 3 varies between Joints 1 and 2. The stroke of the plunger or volume of the air bubbles injected into the water tank $Q_g$ is controlled by the distance between Joints 1 and 3, $L_{13}$.

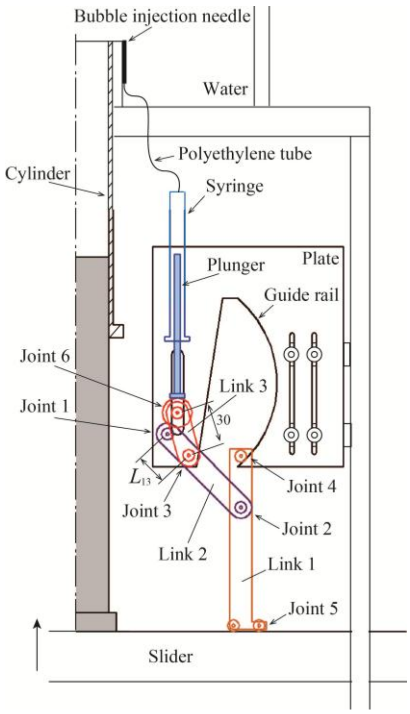


Fig. 5. Device to inject bubbles into water tank.

Joint 4, which is the upper joint of Link 1, moves along the circular-shaped guide rail. Joint 5 of Link 1 and Joint 6 of Link 3 are equipped with pulleys to reduce the friction on the slider and plunger. These mechanisms make the links move more smoothly.

### D. Experimental Condition

The launch of the vortex ring and the injection of the air bubbles are performed under the conditions listed in Table I. The piston velocity for the launch of the vortex ring $U_m$ coincides with the slider velocity. Fig. 6 shows the time variation of the plunger displacement $z_g$ of the bubble injection at the air volume $Q_g/L_0D_0^2 = 2.78 \times 10^{-3}$, where the results at $D_0U_m/\nu = 6630$, 12900, and 19700 are plotted. The displacement at $Q_g/L_0D_0^2 = 0.55 \times 10^{-3}$ is also shown in the case of $D_0U_m/\nu = 19700$. The change in $z_g$ is linear, demonstrating that the air volumetric flow rate $\dot{Q}_g$ $(= \mathrm{d}Q_g/\mathrm{d}t)$ is constant. When compared with the piston displacement $z_p$ of the vortex ring launcher shown in Fig. 3, it is confirmed that the piston moves synchronously with the plunger and that the launch of the vortex ring and the injection of the bubble progress simultaneously.

Fig. 7 shows the relationship between the piston velocity $U_m$ and the air volumetric flow rate $\dot{Q}_g$. The experimental conditions are determined from the specifications of the experimental setup. Since the slider stroke $L_0$ is fixed, the operation time of the slider $T_0$ is determined by $U_m$ and $T_0 \propto L_0/U_m$. Thus, the relationship $\dot{Q}_g \propto Q_g \cdot U_m$ is derived because of $\dot{Q}_g \propto Q_g / T_0$. This relationship is also confirmed by Fig. 7.

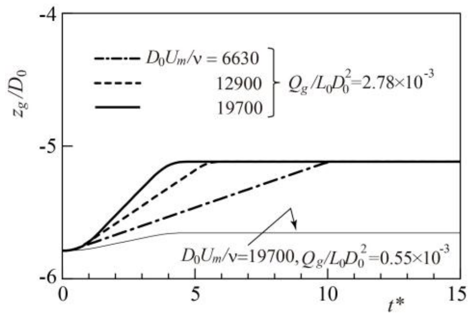


Fig. 6. Displacement profile of plunger.

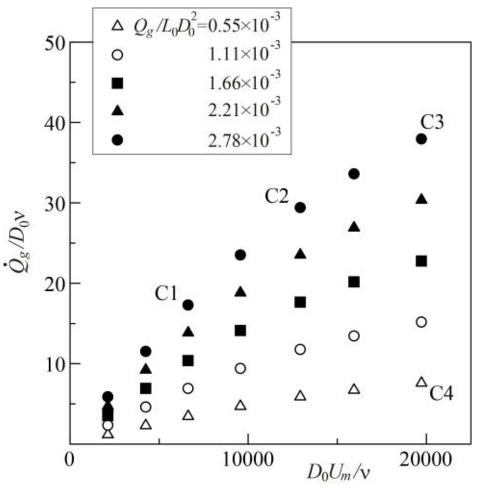


Fig. 7. Experimental condition for bubble injection.

## III. Results and Discussion

### A. Behavior of the Vortex Ring Launched without Air Bubbles

Fig. 8 shows the visualized image of the central vertical cross-section of a vortex ring when no bubbles are injected with the launch of the vortex ring. This is acquired by adding water paint to the launched water in the cylinder. The mean diameter and volume fraction of the paint are 50 μm and 0.006, respectively. A vortex pattern is clearly observed. A shear layer originates at the boundary between the water discharged from the cylinder and still water in the tank, and the paint is entrained in the vortex core with the roll up of the shear layer. A laminar distribution of the paint is found behind the vortex ring, and there are no active mixings. In this study, the laminar vortex rings are observed at every piston velocity $U_m$. The $z$ and $r$ coordinates of the vortex core center are regarded as the displacement and radius of the vortex ring, respectively. The displacement and radius on the same side of the bubble injection needle are denoted by $z_{v1}$ and $r_{v1}$, respectively, and those on the opposite side are denoted by $z_{v2}$ and $r_{v2}$, respectively.

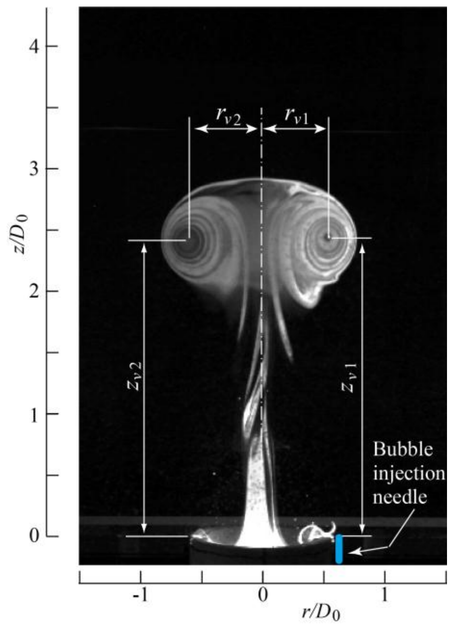


Fig. 8. Visualized image of vortex ring launched without air bubbles ($D_0U_m/\nu = 6630$).

When the vortex ring is launched without the bubble injection, the results of $z_{v1} = z_{v2}$ $(= z_v)$ and $r_{v1} = r_{v2}$ $(= r_v)$ are obtained. Fig. 9 shows the time variation of $z_v$ at the piston velocities $D_0U_m/\nu = 6630$, 12900, and 19700. The time when the piston commences to move is set as $t^* = 0$. The variation of $z_v$ is almost linear, indicating that the vortex ring rises with a constant velocity in still water. The rise almost ceases at $z_v/D_0 \approx 5.8$, because the vortex ring is affected by the water surface at $z/D_0 = 6$.

The radius $r_v$ is plotted against the displacement $z_v$ in Fig. 10. The radius remains nearly unaltered at $z_v/D_0 \leqq 5.8$. The marked increase at $z_v/D_0 > 5.8$ is attributable to the water surface effect.

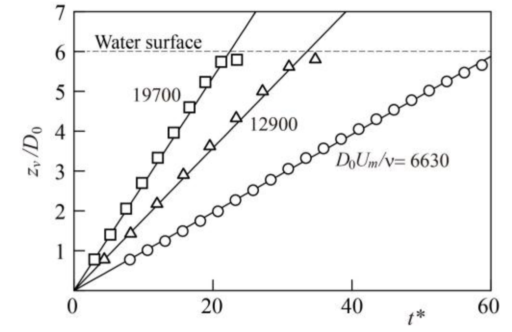


Fig. 9. Time variation of displacement for vortex ring launched without air bubbles.

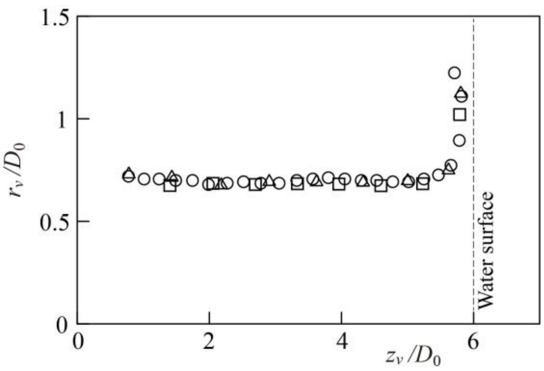


Fig. 10. Change in radius of vortex ring launched without air bubbles.

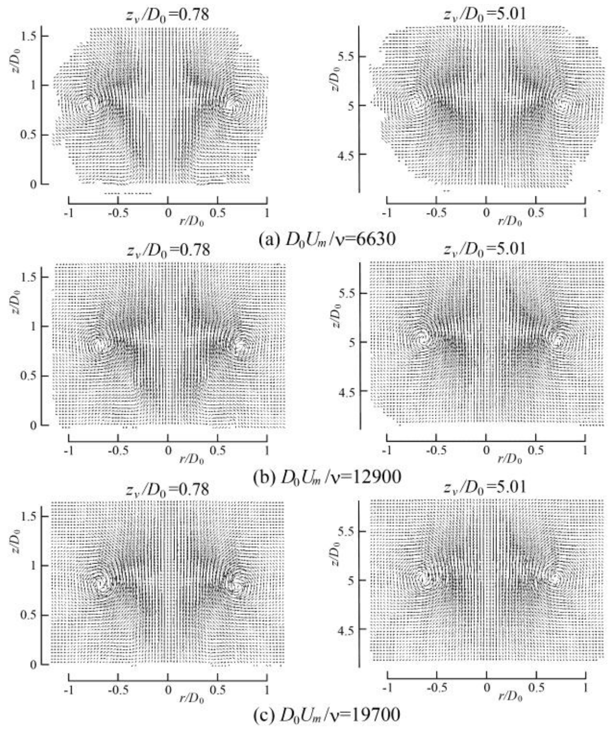


Fig. 11. Water velocity distribution on vertical cross-section passing through the cylinder centerline when no bubbles are released.

This study measures the water velocity $\boldsymbol{u}$ with a PIV system on the central vertical cross-section of the vortex ring at the displacements of $z_v/D_0$ = 0.78, 2.77, 4.1, and 5.01. The ensemble-averaged velocity $\hat{\boldsymbol{u}}$ is calculated on the basis of the velocity $\boldsymbol{u}$ measured by 10 experiments. Fig. 11 shows the distribution of $\hat{\boldsymbol{u}}$ around the vortex cores at $z_v/D_0$ = 0.78 and 5.01. The bubbles are not released. The distributions for the piston velocities at $D_0U_m/\nu$ = 6630, 12900, and 19700 are plotted. The vortex core is nearly circular, and the velocity distribution barely depends on the displacement of the vortex ring. The vortex ring almost maintains its strength with the convection.

The vorticity is calculated from the ensemble-averaged velocity $\hat{\boldsymbol{u}}$ by the second-order finite difference scheme and the circulation $\Gamma$ of the vortex ring is computed from the distribution. Fig. 12 shows the relationship between $\Gamma$ and the displacement of the vortex ring. The circulation or strength of the vortex ring is nearly constant. The circulation $\Gamma$ is slightly larger than the $\Gamma_0$ estimated from Eq. (1) presented by Glezer [15]. Such a difference was also reported by the experiments of Glezer [15] and Gharib *et al.* [16]. Equation (1) is based on a slug flow model that assumes the water on the cross-section of the cylinder has a uniform velocity. The difference between $\Gamma$ and $\Gamma_0$ is attributable to this assumption.

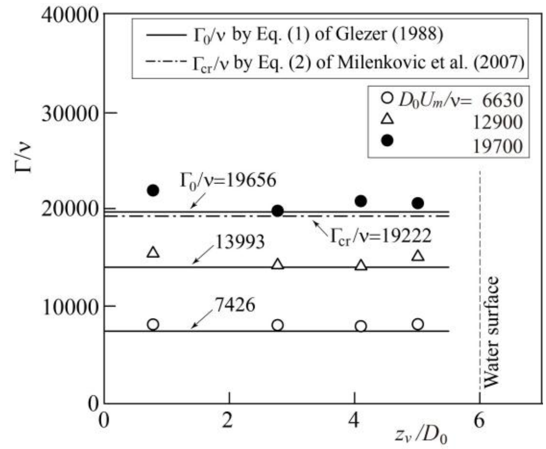


Fig. 12. Change in circulation of vortex ring launched without air bubbles.

## B. Motion of the Bubbles Injected into Still Water

Fig. 13 shows the motion of air bubbles injected into still water, and the results for conditions C1, C2, C3, and C4 indicated in Fig. 7 are depicted. These conditions yield specific flow patterns when a vortex ring is launched with the bubbles, as explained later. At conditions C1, C2, and C3, the injected air volume $Q_g/L_0D_0^2$ is $2.78 \times 10^{-3}$. Fig. 13 (a) shows the results for condition C1, in which the air volumetric flow rate $\dot{Q}_g$ is the lowest. The bubbles rise almost vertically just after their injection, forming a long train. When the air flow rate increases (condition C2), the bubbles form a cluster at a certain height, as seen in Fig. 13 (b). When the air flow rate increases further (condition C3), the time period for the bubble injection is the shortest and the vertical distance between the bubbles is small. Consequently, the bubble cluster appears just after the bubble injection. For condition C4, the injected bubble volume is lower ($Q_g/L_0D_0^2 = 0.55 \times 10^{-3}$). While the bubbles rise vertically just after their injection, they form a cluster at a certain height.

The bubble diameter $d_b$ measured at the bubble injection needle outlet is plotted against the slider velocity $U_m$ in Fig. 14. $d_b$ is not dependent on the injection conditions and the mean diameter is 3.4 mm.

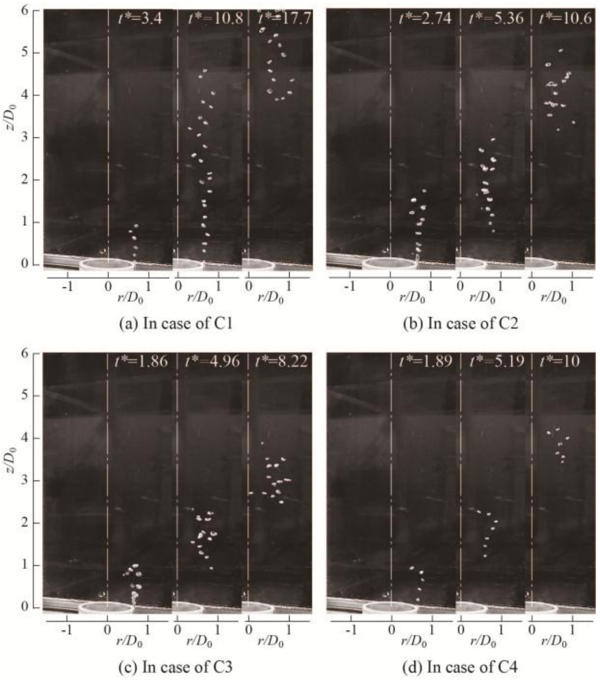


Fig. 13. Motion of bubbles injected into still water.

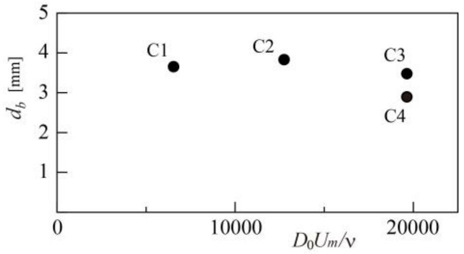


Fig. 14. Mean bubble diameter in still water.

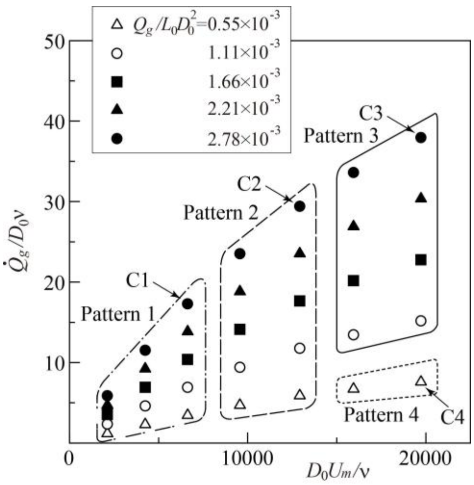


Fig. 15. Classification of bubble motion relative to vortex ring.

### C. Entrainment and Transport of Bubbles by a Vortex Ring

The behavior of the vortex ring and the bubble motion are classified into four patterns according to their visualizations. They depend on the piston velocity $U_m$ and the air volumetric flow rate $\dot{Q}_g$, as illustrated in Fig. 15. The visualized images for conditions C1, C2, C3, and C4 are discussed. The vertical cross-section of the vortex core is visualized with water paints. Fig. 16 shows the vortex ring and the bubbles for condition C1 ($D_0U_m/\nu$ = 6630, $Q_g/L_0D_0^2$ = 2.78 $\times 10^{-3}$). When $t^* \leqq 6.29$, the water inside the cylinder and the air in the syringe are flowing into the water tank, because the slider is in a vertical motion. In case the vortex ring is not launched, the bubbles rise almost vertically just after their injection as shown in Fig. 13 (a). In the case where the vortex ring is launched, the vortex core makes the bubbles move in a radial direction at $t^*$ = 3.4 and 6.29, but the bubbles rise without being entrained in the vortex core. At $t^* \geqq 10.8$, all the injected bubbles rise to a position higher than the vortex ring. In condition C1, the bubbles are not entrained in the vortex core and rise via the buoyant force.

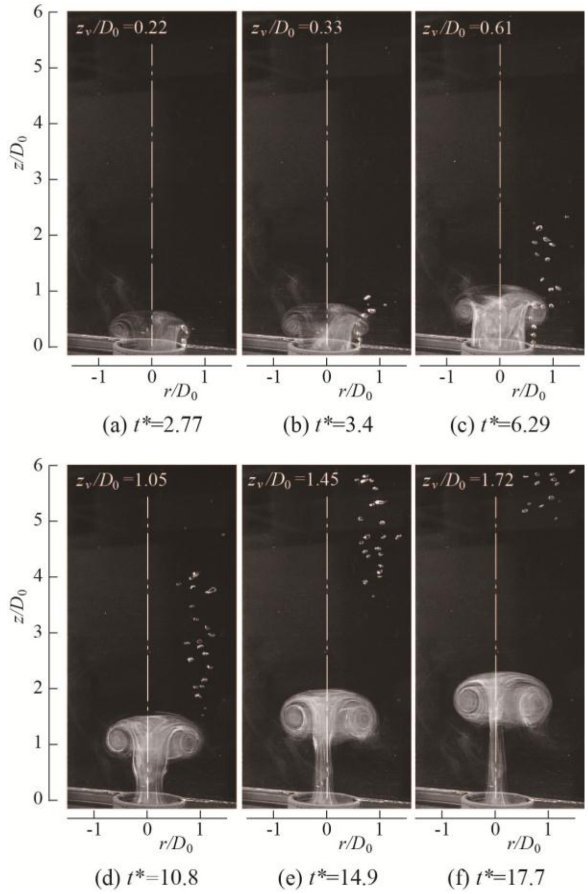


Fig. 16. Bubble motion and behavior of vortex ring at condition C1.

Fig. 17 shows the results for condition C2 ($D_0U_m/\nu$ = 12900, $Q_g/L_0D_0^2$ = 2.78 $\times 10^{-3}$). The piston velocity $U_m$ is higher than that for condition C1. When $t^*$ = 0.73, the bubbles injected at the beginning of the injection period rise to a position higher than the vortex ring, but the subsequently injected bubbles rise with being entrained in the vortex core. The entrainment is caused by a pressure gradient induced by the water vortical motion. The bubbles entrained in the vortex ring circumferentially disperse around the vertical ($z$) axis of the vortex ring, as seen in the images at $t^*$ = 2.74 and 5.36. The bubbles injected in the latter half of the injection period pass through the vortex core at $t^*$ =5.36 and rise to the upper region at $t^*$ =10.6. This is because the bubbles are accelerated by the buoyant force before reaching the vortex core, resulting in a higher rising velocity. At $t^* \geqq 17.9$, the bubbles inside the vortex core separate from the vortex core and rise with a higher velocity compared with the vortex ring. This is because the buoyant force becomes more dominant than the pressure gradient force holding the bubbles in the vortex core. There are no bubbles inside the vortex core at $t^*$ = 28.

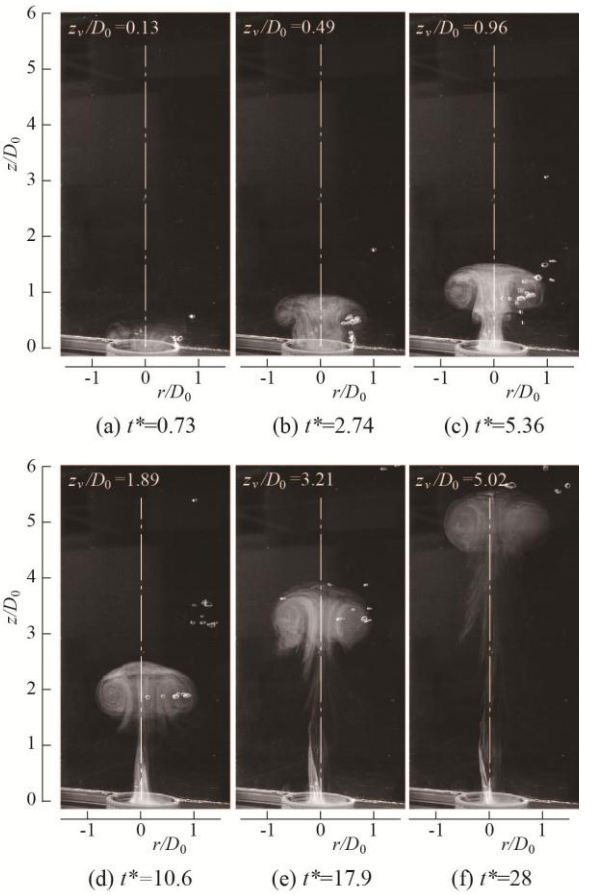


Fig. 17. Bubble motion and behavior of vortex ring at condition C2.

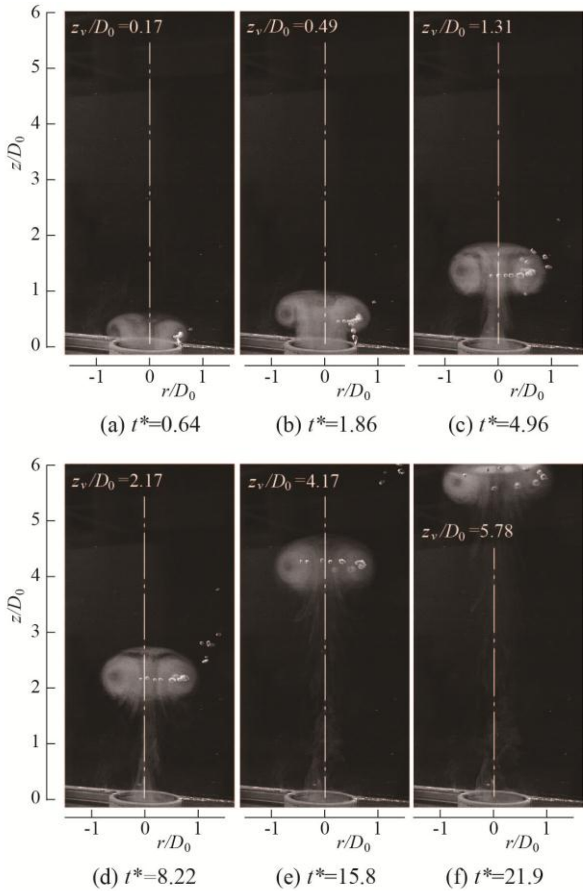


Fig. 18. Bubble motion and behavior of vortex ring at condition C3.

Fig. 18 shows the vortex ring and the bubbles for condition C3 ($D_0U_m/\nu$ = 19700, $Q_g/L_0D_0^2$ = 2.78 × $10^{-3}$). The piston velocity $U_m$ is further increased. The bubbles are entrained in the vortex core except for those injected at the beginning of the injection period, as seen in the images at $t^* \leqq 4.96$. Because the strength of the vortex ring is higher, the bubbles widely distribute around the vertical ($z$) axis of the vortex ring. At $t^*$ = 4.96, some of the bubbles injected in the latter half of the injection period exist in a location slightly off from the center of the vortex core. These bubbles are separated from the vortex core at $t^*$ = 8.22; however, bubble separation from the vortex core does not occur at $t^* \geqq 8.22$. The entrained bubbles rise with the vortex ring. Most of the bubbles injected in the water are transported to the water surface with the vortex ring.

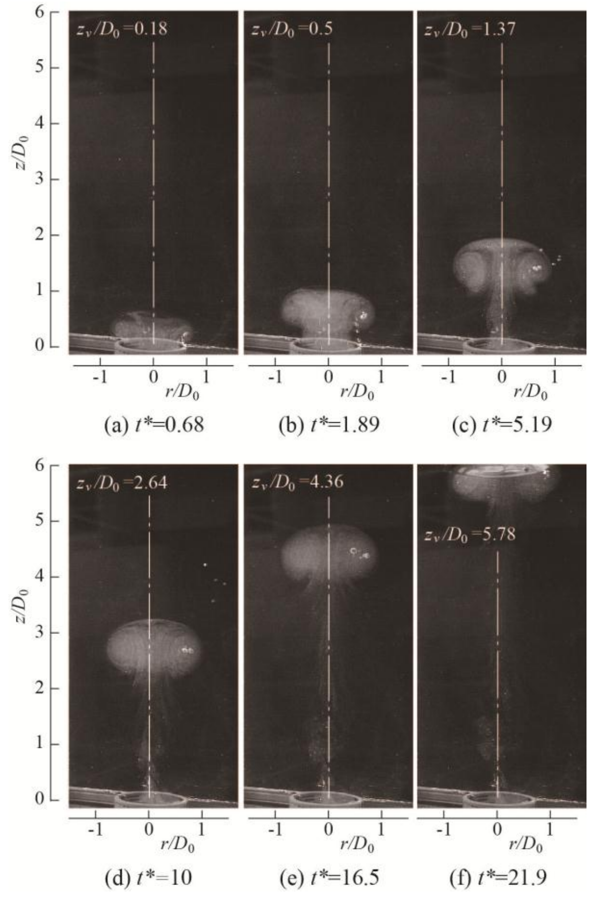


Fig. 19. Bubble motion and behavior of vortex ring at condition C4.

Fig. 19 shows the results for condition C4 ($D_0U_m/\nu$ = 19700, $Q_g/L_0D_0^2$ = 0.55 × $10^{-3}$). The piston velocity $U_m$ is the same as that for condition C3, but the bubble volume is reduced to 1/5. All the injected bubbles are entrained in the vortex core, as seen in the images at $t^* \leqq 5.19$. This is because the flow rate and rising velocity of the bubbles are lower. Though some bubbles are separated from the vortex core at $t^*$ = 10, there are no bubbles separating from the vortex core after.

According to the visualized images of the vertical cross-section of the vortex ring, the displacements $z_{v1}$ and $z_{v2}$ of the vortex ring are the same even when the bubbles are injected. They are denoted by $z_v$. Fig. 20 shows the bubble distribution relative to the vortex core, where the center of the vortex core on the same side of the bubble injection needle is set at the origin of the coordinates. For conditions C3 and C4, it is confirmed that a number of bubbles are entrained in the vortex core and that they are transported by the convection of the vortex ring.

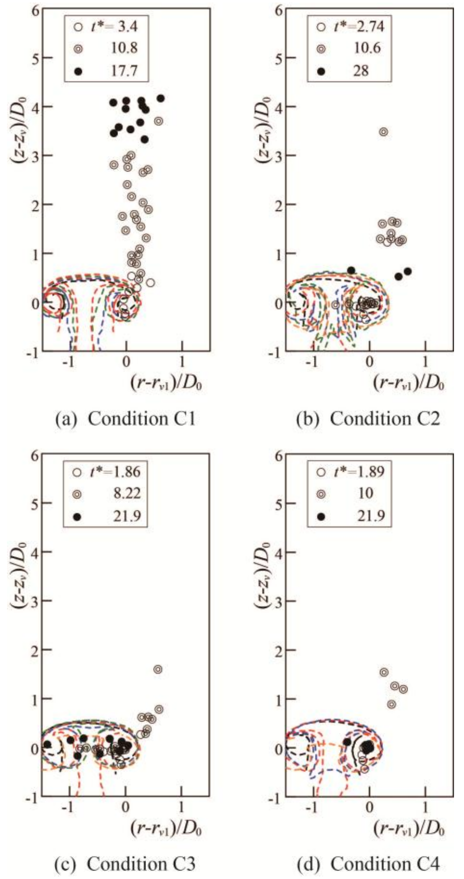


Fig. 20. Bubble motion relative to vortex ring (The vertical cross-section of the vortex ring is outlined at three time points).

When the number of bubbles inside the vortex core $n$ is measured in the region visualized with white paints, it changes with the displacement of the vortex ring $z_v$, as shown in Fig. 21. $n_0$ is the number of bubbles injected from the needle. The bubbles are scarcely entrained in the vortex core in condition C1. For condition C2, the bubbles injected at the beginning of the injection period are entrained, and they are separated from the vortex ring by the convection of the vortex ring. Therefore, the number of bubbles markedly decreases at the displacement $z_v/D_0 \geqq 2$. Conditions C3 and C4 both successfully achieve the bubble entrainment and transport. More than 60% of the bubbles injected into the water are entrained in the vortex core and transported a distance five times larger than the cylinder diameter $D_0$.

The time variation of the displacement for the vortex ring $z_v$ is shown in Fig. 22, where the results for the bubble-free condition are also plotted. The bubbles barely affect the displacement.

Fig. 23 shows the radii $r_{v1}$ and $r_{v2}$. For conditions C2 and C3, $r_{v1}$ is larger than $r_{v2}$. This is because the bubbles entrained in the vortex core move in the radial direction, swirling around the center of the vortex core and enlarging the vortex core in that direction. This remarkable enlargement occurs in condition C2 because the strength of the vortex ring is lower. The bubble effect is small for condition C4 owing to the lower bubble volume.

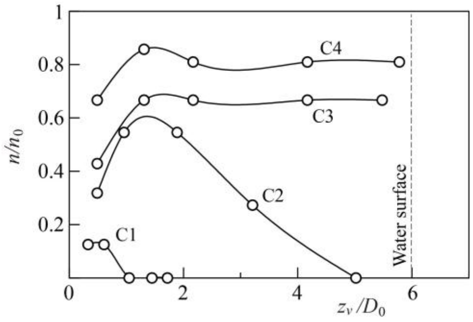


Fig. 21. Change in number of bubbles inside vortex core.

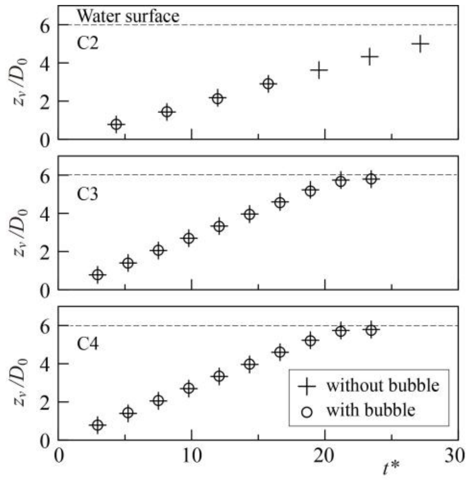


Fig. 22. Time variation of displacement for vortex ring at conditions C2, C3, and C4.

### *D. Circulation for Generation and Transport of Bubble Clusters*

Milenkovic *et al.* [17] experimentally and theoretically investigated the entrainment of a single bubble in a vortex ring appearing around the central axis of a bubbly jet issued vertically upward from a circular nozzle. They derived the condition under which a bubble with diameter $d_b$ and terminal velocity $V_t$ can be entrained in a vortex core with a vorticity $\omega_{cr}$ and a radius $R_v$ as follows;

$$\mathrm{Fr}_\omega \geq \frac{\mathrm{Fr}_b \beta}{\left(0.135\mathrm{Fr}_b^2 \beta^2 + 0.01\right)^{1/2}} \tag{2}$$

where $\mathrm{Fr}_\omega$ is the Froude number of the vortex core, $\mathrm{Fr}_b$ is the Froude number of the bubble, and $\beta$ is the length scale ratio. These are defined as

$$\mathrm{Fr}_\omega = \frac{\omega_{cr}^2 R_v}{4g}, \quad \mathrm{Fr}_b = \frac{V_t^2}{2gd_b}, \quad \beta = \frac{d_b}{2R_v} \tag{3}$$

In this study, the measured results at the outlet of the bubble injection needle are $d_b$ = 0.0034 m, $V_t$ = 0.23 m/s and $R_v$ = 0.009 m. Consequently, the minimum circulation $\Gamma_{cr}$ (= $\pi R_v^2 \omega_{cr}$ ) of a vortex ring entraining the bubbles is calculated as $\Gamma_{cr} / \nu$ = 19222 from Eq. (2). The $\Gamma_{cr}$ value is superimposed by a chain line in Fig. 12. The circulations $\Gamma$ at the piston velocity $D_0 U_m/\nu$ = 19700 plotted by the circular painted symbols are almost parallel with $\Gamma_{cr}$. The piston velocity corresponds to conditions C3 and C4, in which the bubbles are entrained in the vortex core and transported by the vortex ring. Therefore, one can find that Eq. (2), proposed by Milenkovic *et al.* [17], is also applicable to the prediction of the circulation that allows the vortex ring to generate and transport a bubble cluster in this study.

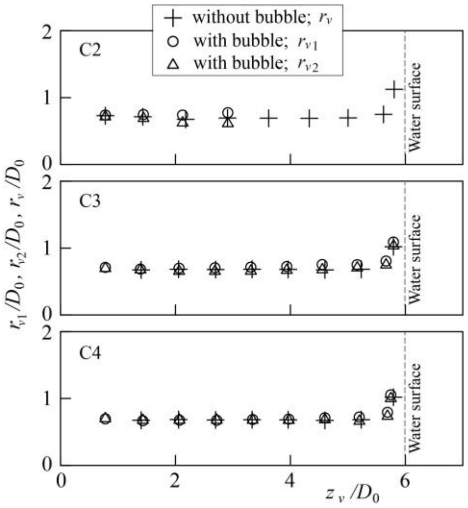


Fig. 23. Change in radius of vortex ring at conditions C2, C3, and C4.

## IV. Conclusions

The possibility of generation and transport of a bubble cluster by a vortex ring in water is explored experimentally. A vortex ring is launched vertically upward into a water tank by discharging the water in a cylinder mounted at the bottom of the tank with a piston. Air bubbles are successively injected into the vortex ring from a needle attached to the cylinder outlet. The cylinder inner diameter $D_0$ and the piston stroke $L_0$ are 42.5 mm and 100 mm, respectively. The circulation of the vortex ring is less than 20000, and accordingly laminar vortex rings are launched. The mean diameter of the bubbles is 3.4 mm, and the air volume is less than 2.78 x $10^{-3}L_0D_0^2$. The behavior of the vortex ring and the bubble motion are investigated. The results are summarized as follows:

1) The bubble motion relative to the vortex ring can be classified into four patterns according to the piston velocity (strength of the vortex ring) and the air volumetric flow rate.
2) In Pattern 1, the injected bubbles rise via the buoyant force without being entrained in the vortex core.
3) In Pattern 2, the bubbles injected in the first half of the injection period rise while being entrained in the vortex core. The entrained bubbles circumferentially disperse around the vertical axis of the vortex ring, and they are separated from the vortex core by the convection of the vortex ring. The bubbles injected in the latter half of the injection period rise independent of the vortex ring.
4) In Pattern 3, the bubbles, except for those injected at the beginning of the injection period, are entrained in the vortex core and they circumferentially distribute around the vertical axis of the vortex ring. The entrained bubbles rise with the vortex ring.
5) In Pattern 4, all the bubbles are entrained into the vortex core. A part of them are separated, but most of them rise with the vortex ring.
6) The entrained bubbles barely affect the displacement of the vortex ring; however, they make the radius of the vortex ring larger.
7) The formula proposed by Milenkovic *et al.*, which gives the circulation of a vortex ring entraining a single bubble in the vortex core, predicts the circulation of a vortex ring that entrains and transports air bubbles under the experimental conditions of this study.

## Appendix

$d_b$ : diameter of bubble
$D_0$: inner diameter of cylinder
$\mathrm{Fr}_b$ : Froude number of bubble
$\mathrm{Fr}_\omega$ : Froude number of vortex core
$g$: gravitational constant
$L_0$: stroke of piston
$n$: number of bubbles in vortex core
$n_0$: number of bubbles injected into water
$Q_g$: volume of bubbles injected into water
$\dot{Q}_g$ : air volumetric flow rate = $\mathrm{d}Q_g/\mathrm{d}t$
$r$: radial coordinate
$r_v$: radius of vortex ring
$R_v$: radius of vortex core
$t$: time
$t^*$: non-dimensional time = $t(g/D_0)^{1/2}$
$T_0$: operation time of piston and syringe
$U_0$: velocity of piston
$U_m$: maximum value of $U_0$
$\boldsymbol{u}$: velocity of water
$\hat{\boldsymbol{u}}$ : ensemble-averaged value of $\boldsymbol{u}$
$V_t$: bubble terminal velocity
$z$: axial coordinate
$z_g$: displacement of plunger
$z_p$: displacement of piston
$z_v$: displacement of vortex ring
$\beta$: length scale ratio
$\Gamma$: circulation
$\Gamma_0$: circulation of vortex ring at launch, Eq. (1)
$\Gamma_{cr}$: minimum circulation entraining bubble
$\nu$: kinematic viscosity of water

Subscripts
1: on the same side of bubble injection needle
2: on the opposite side of bubble injection needle

## References

[1] K. Domon, O. Ishihara, and S. Watanabe, "Mass transport by a vortex ring," *J. Phys. Soc. Japan*, vol. 69, pp.120-123, 2000.
[2] H. Yagami and T. Uchiyama, "Numerical simulation for the transport of solid particles with a vortex ring," *Advanced Powder Technology*, vol. 22, pp.115-123, 2011.
[3] C. T. Crowe, J. N. Chung, and T. R. Troutt, "Particle mixing in free shear flows," *Prog. Energy Combust. Sci.*, vol. 14, pp.171-194, 1988.
[4] O. A. Druzhinin and S. E. Elghobashi, "Direct numerical simulation of a three-dimensional spatially developing bubble-laden mixing layer with two-way coupling," *J. Fluid Mech.*, vol. 429, pp.23-61, 2001.
[5] G. R. Ruetsch and E. Meiburg, "Two-way coupling in shear layers with dilute bubble concentrations," *Phys. Fluids*, vol. 6, pp.2656-2670, 1994.

[6] G. Sridhar and J. Katz, "Drag and lift forces on microscopic bubbles entrained by a vortex," *Phys. Fluids*, vol. 7, pp. 389-399, 1995.

[7] G. Sridhar and J. Katz, "Effect of entrained bubbles on the structure of vortex rings," *J. Fluid Mech.*, vol. 397, pp. 171-202, 1999.

[8] F. J. Higuera, "Axisymmetric inviscid interaction of a bubble and a vortex ring," *Phys. Fluids*, vol. 16, pp.1156-1159, 2004.

[9] T. Uchiyama, "Three-dimensional vortex simulation of bubble dispersion in excited round jet," *Chem. Eng. Sci.*, vol. 59, pp. 1403-1413, 2004.

[10] T. Uchiyama and Y. Yoshi, "Numerical study of the entrainment and transport of gas bubbles by a vortex ring," *J. Chem. Eng. & Process Technol.*, vol. 6, Article ID 245, 2015.

[11] Z. Wang, T. Uchiyama, and B. Chen, "Numerical simulation of the interaction between vortex ring and bubble plume," *Applied Mathematical Modelling*, vol. 37, pp. 10007-10026, 2013.

[12] T. Uchiyama and S. Kusamichi, "Interaction of bubbles with vortex ring launched into bubble plume," *Advances in Chem. Eng. Sci.*, vol. 3, pp. 207-217, 2013.

[13] Y. Abe, M. Kawaji, and T. Watanabe, "Study on the bubble motion control by ultrasonic wave," *Exp. Therm. Fluid Sci.*, vol. 26, pp. 817-826, 2002.

[14] Y. Tanaka, R. Suzuki, K. Arai, K. Iwamoto, and K. Kawazura, "Visualization of flow fields in a bubble eliminator," *J. Visualization*, vol. 4, pp. 81-90, 2001.

[15] A. Glezer, "The formation of vortex rings," *Phys. Fluids*, vol. 31, pp. 3532-3542, 1988.

[16] M. Gharib, E. Rambod, and K. Shariff, "A universal time scale for vortex ring formation," *J. Fluid Mech.*, vol. 360, pp.121-140, 1998.

[17] R. Milenkovic, B. Sigg, and G. Yadigaroglu, "Bubble clustering and trapping in large vortices, Part 1: Triggered bubbly jets investigated by phase-averaging," *Int. J. Multiphase Flow*, vol. 33, pp.1088-1110, 2007.


**Tomomi Uchiyama** was born in Shizuoka Prefecture, Japan, in 1962. He finished the Graduate School of Engineering, Nagoya University, Japan in 1987, and received his degree, Dr. Eng., from Nagoya University in 1992. He is a professor at Institute of Materials and Systems for Sustainability, Nagoya University, Japan. His current research interest lies in fluid engineering, especially CFD, multi-phase flow, and micro-hydraulic turbine.

**Sou Kusamichi** was born in Kagoshima Prefecture, Japan, in 1986. He finished the Graduate School of Information Science, Nagoya University, Japan in 2011. He is an engineer at Bridgestone Cycle Co., Ltd, Japan.